9th IFAC Conference on Control Applications in Marine Systems
The International Federation of Automatic Control
September 17-20, 2013. Osaka, Japan

Exhaust Gas Recirculation Control for Large Diesel Engines - Achievable Performance with SISO Design

Jakob Mahler Hansen [*,**] **Mogens Blanke** [*,***]
Hans Henrik Niemann [*] **Morten Vejlgaard-Laursen** [**]

[*] *Department of Electrical Engineering, Technical University of Denmark, Kgs. Lyngby, Denmark*
[**] *MAN Diesel & Turbo, Copenhagen SV, Denmark*
[***] *AMOS CoE, Institute of Technical Cybernetics, Norwegian University of Science and Technology, Trondheim, Norway*

Abstract: This paper investigates control possibilities for Exhaust Gas Recirculation (EGR) on large diesel engines. The goal is to reduce the amount of NO_x in the exhaust gas by reducing the oxygen concentration available for combustion. Control limitations imposed by the system are assessed using linear analysis of the highly non-linear dynamics. Control architectures are investigated and performance in terms of disturbance rejection and reference tracking are investigated under model uncertainty. Classical feed-forward and feedback controller designs are investigated using classical and Quantitative Feedback Theory (QFT) designs. Validation of the controller is made on the model with focus on disturbance reduction ability.

Keywords: Exhaust gas recirculation; Diesel engine; Green ship; Robust; Qualitative Feedback.

1. INTRODUCTION

Exhaust Gas Recirculation (EGR) can reduce engine emissions through reduction of O_2 concentration in the air intake to combustion engines. This paper considers control of the EGR process on a large two-stroke diesel engine with focus on the control challenges in this process and the obtainable performance. This paper addresses single input single output (SISO) methods.

Due to environmental concerns, the International Maritime Organization (IMO) has issued a series of protocols limiting the emission permitted by diesel engines. The protocols are called Tier I, II, and III, and concern the emission of NO_x, SO_x and greenhouse gasses. The Tier I and II protocols are global limits and have taken effect in 2000 and 2011 respectively. The Tier III protocol applies to NO_x in Emission Control Areas from 2016.

The EGR technology reuses the engine exhaust gas in the combustion in order to reduce the amount of oxygen in the engine intake and thereby reduce the amount of NO_x created in the engine. There is an upper limit for how much exhaust gas can be recirculated without depriving the engine of sufficient oxygen for the combustion.

The majority of scientific literature on EGR technology deals with four-stroke automotive engines. The very non-linear dynamics of the EGR process is difficult to model but good fits to real data have been demonstrated by Wahlström and Eriksson [2011b] for truck engines. Model-based feedback has been attempted by several researchers Alfieri et al. [2006], Chen and Wang [2012], but these approaches need very accurate models over the range of operation. Robust control was in focus in Colin et al. [2011] using linear constant parameter controls showing which performance is achievable with linear methods for driving conditions. Control dealing with both variable geometry turbine and EGR was recently treated in Wang et al. [2011a,b] using linear robust design. Good results with non-linear methods were shown in Kotman et al. [2010], Wahlström and Eriksson [2011a], but non-linear dynamic models are needed with an accuracy not available for large two-stroke engines.

This paper first introduces an experimentally verified non-linear model. The model is investigated for uncertainty presented by model parameters. Control architectures based on classical control and then designed and supplemented by Quantitative Feedback Theory (QFT) methods to cope with robustness issues.

2. MODEL

The engine in the EGR-system is a two-stroke diesel 4T50ME-X engine with four cylinders. The air intake for the engine is supplied by a Variable Geometry Turbocharger (VGT), consisting of a compressor and a turbine on a common shaft. The exhaust gas of the engine passes through the turbine, which in turn drives the compressor, supplying pressurised ambient air to the engine.

There are two manifolds in the system where pressures are measured: a scavenge air manifold is located at the engine intake; an exhaust air manifold is located at the output of the engine. Scavenge pressure has to be higher than the exhaust pressure for two-stroke engines.

The EGR-loop connects the two manifolds, where a blower provides a mass flow from exhaust to scavenge manifold.

The exhaust gas passes through a scrubber, a cooling unit, a blower, and a valve. It has to be ensured that the blower rotates sufficiently fast to overcome the pressure ratio between the manifolds.

The two cooling units in the model are assumed to ideally decrease the temperature of the incoming gas to the indicated level, without affecting the mass flow.

The input signals are: the opening of the Change-Over-Valve (COV), u_{egr}, and the speed of the EGR-blower, ω_{blow}. The disturbances are; the opening of the VGT, u_{vgt}, and the engine load, u_{load}. The primary control variable of the engine, the engine load, which is used to control the revolutions of the engine torque and hence the shaft speed, is considered a measured disturbance. It is desired to control the scavenge oxygen concentration, O_{scav}.

An illustration of the engine model is shown in Fig. 1, where inputs and disturbances are marked with inclined arrows. The signals measured on the engine are underlined.

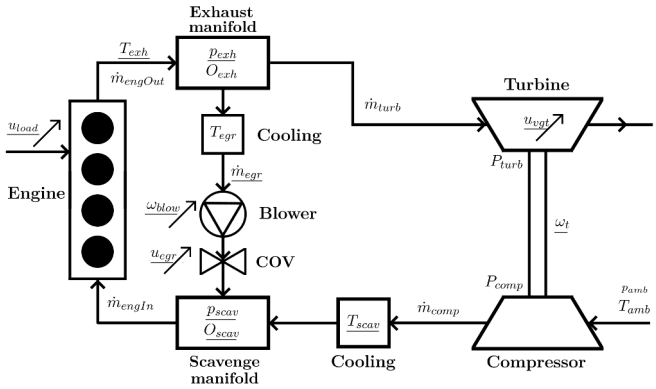

Fig. 1. Model structure of the EGR system. There are two control inputs (u_{egr} and ω_{blow}) and two inputs (u_{vgt} and u_{load}) that are measured disturbances.

2.1 Non-linear state space model

A non-linear state space model has been derived consisting of seven differential equations and two difference equations. The nine states can be seen in Table A.1. The two discrete states originate from exhaust gas temperature expressions as suggested by Wahlström and Eriksson [2011b].

The main findings on the modelling of the engine system is summarised here, see Hansen et al. [2013] for a detailed model description. The engine mass flow intake has been modelled as the mass flow through a restriction. The mass flows through the compressor and turbine have been least-squares fitted to maps by use of polynomials. The mass flow through the EGR-loop is modelled as the mass flow through a compressor with variable opening. Differential equations were used to describe the pressures and oxygen concentrations in the two manifolds.

2.2 Model fit

The response of the non-linear model has been compared to the measured signals from the 4T50ME-X diesel engine. Fig. 2 shows the oxygen concentration in the scavenge manifold where the engine load of changes from 35% to 75% at time 2000 seconds.

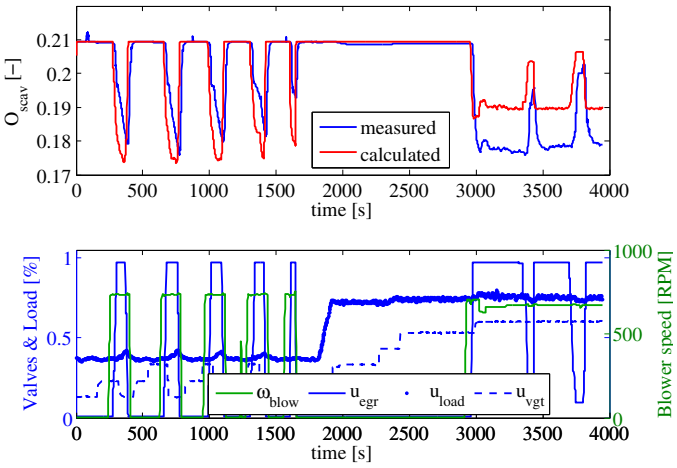

Fig. 2. Comparison of the measured and modelled oxygen concentration in the scavenge manifold

The model fits the measurement well for engine loads around 35%, which is the lowest engine load for the system configuration, and for loads of 100%. An offset in O_2 has been observed at engine load 75%, however, it is assumed that a better fit could be obtained for this region with more data available.

2.3 Transfer function model

The non-linear model is linearised around an operation point for 35% engine load. The linear model is represented on transfer function form, describing the transition from inputs and disturbances to the output, see Fig. 3

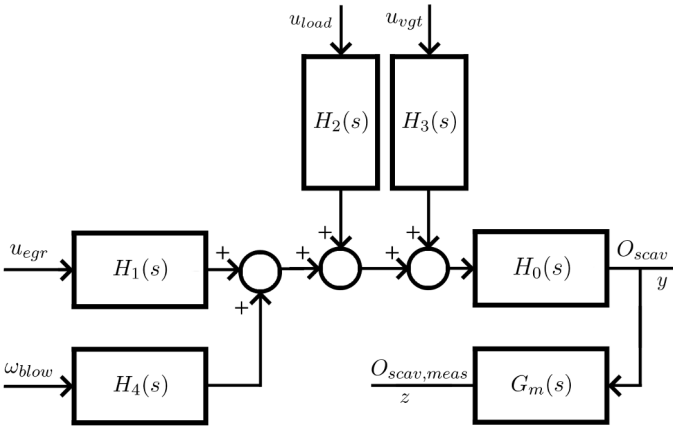

Fig. 3. Transfer function model with two control inputs (u_{egr} and ω_{blow}), two disturbance inputs (u_{vgt} and u_{load}) and a measurement delay $\boldsymbol{G}_m(s)$

The common dynamics of the inputs and disturbances are collected in $\boldsymbol{H}_0(s)$. The model experiences a measurement delay denoted $\boldsymbol{G}_m(s) = e^{-\tau_d s}$. It is assumed that $\tau_d = 5[s]$. The model is given as:

$$z = \boldsymbol{H}_0 \begin{bmatrix} \boldsymbol{H}_1 & \boldsymbol{H}_4 \end{bmatrix} \begin{bmatrix} u_{egr} \\ \omega_{blow} \end{bmatrix} + \boldsymbol{H}_0 \begin{bmatrix} \boldsymbol{H}_2 & \boldsymbol{H}_3 \end{bmatrix} \begin{bmatrix} u_{load} \\ u_{vgt} \end{bmatrix} \quad (1)$$

$$y = \boldsymbol{G}_m \boldsymbol{H}_0 \begin{bmatrix} \boldsymbol{H}_1 & \boldsymbol{H}_4 \end{bmatrix} \begin{bmatrix} u_{egr} \\ \omega_{blow} \end{bmatrix} + \boldsymbol{G}_m \boldsymbol{H}_0 \begin{bmatrix} \boldsymbol{H}_2 & \boldsymbol{H}_3 \end{bmatrix} \begin{bmatrix} u_{load} \\ u_{vgt} \end{bmatrix} \quad (2)$$

Since the two inputs almost have the same dynamics the controllers designed for the model will focus on a SISO model where u_{egr} is kept constant, leaving $u = \omega_{blow}$. Likewise, only one disturbance is considered, $d = u_{load}$, where u_{vgt} is held constant.

The simplified model with two transfer functions given as; $\boldsymbol{G}(s) \triangleq \boldsymbol{H}_4(s)\boldsymbol{H}_0(s)$ and $\boldsymbol{G}_d(s) \triangleq \boldsymbol{H}_2(s)\boldsymbol{H}_0(s)$, are scaled to have a DC-gain of unity. This results in the two scaled transfer functions, linearised for 35% load,

$$\boldsymbol{G} = \frac{-10.86(s^2 + 0.59s + 0.13)}{(s + 9.92)(s + 1.56)(s + 0.48)(s + 0.19)} \quad (3)$$

$$\boldsymbol{G}_d = \frac{-0.76(s + 11.54)(s + 0.16)}{(s + 9.92)(s + 1.56)(s + 0.48)(s + 0.19)} \quad (4)$$

The transfer functions are depicted in the Bode plot in Fig. 4 along with the approximate frequency interval of sea-waves. As the waves impact the propeller load and the engine's shaft speed control (governor) will react to this through corrective adjustments to the fuel flow, the input d will fluctuate at wave frequencies. The controller should therefore both be robust to parameter uncertainty and variations over the envelope of operation and it is desired that it is also able to reject disturbances in the wave frequency range. Using different linearisation points the model transfer function changes. For linearisation around 50% and 75% engine load the model is:

$$\boldsymbol{G}_{50\%} = \frac{-11.29(s^2 + 0.67s + 0.18)}{(s + 10.08)(s + 1.63)(s + 0.52)(s + 0.25)} \quad (5)$$

$$\boldsymbol{G}_{75\%} = \frac{-11.56(s^2 + 0.70s + 0.22)}{(s + 10.12)(s + 1.67)(s + 0.53)(s + 0.30)} \quad (6)$$

these transfer functions are also shown in Fig. 4.

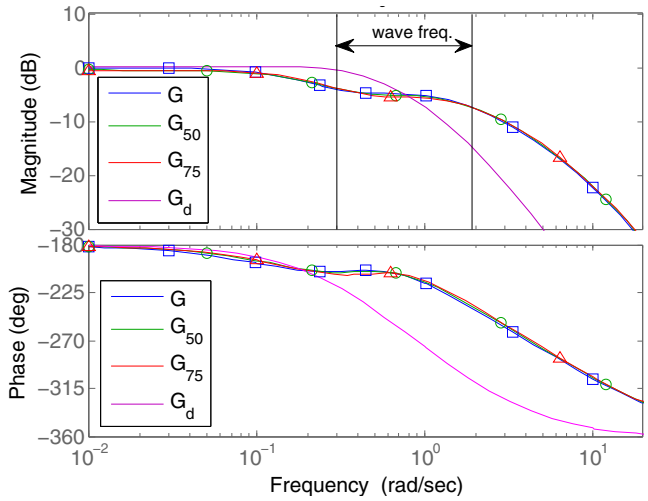

Fig. 4. Bode plot of $\boldsymbol{G}(s)$ and $\boldsymbol{G}_d(s)$. Wave frequency interval is indicated with black lines. The linearisations are marked as; □ for $\boldsymbol{G}$, ○ for $\boldsymbol{G}_{50\%}$ and △ for $\boldsymbol{G}_{75\%}$.

Particular control effort is seen to be needed if disturbances shall be suppressed for frequencies in the wave-interval and a decade below, as $|\boldsymbol{G}(j\omega)| < |\boldsymbol{G}_d(j\omega)|$ in this frequency region. The difference between the three linearisations is small.

2.4 Model uncertainty

The controlled model is desired to be robust towards uncertainty of model parameters. Model uncertainty is investigated by varying specific model parameters, here the cross sectional engine opening, A_{eng}. The parameter, A_{eng}, represents the uncertainty of the mass flow calculations. A complete list of model parameters can be found in Hansen et al. [2013]. Fig. 5 and 6 shows the bodeplots for $\boldsymbol{G}(s)$ and $\boldsymbol{G}_d(s)$, respectively, for different gains on the A_{eng}-parameter. The gains will be used for legends in subsequent plots. The gain of 1 denotes nominal value. In the sequel, the nominal model transfer functions are denoted $\bar{\boldsymbol{G}}(s)$, $\bar{\boldsymbol{G}}_d(s)$ and $\bar{\boldsymbol{G}}_m(s)$.

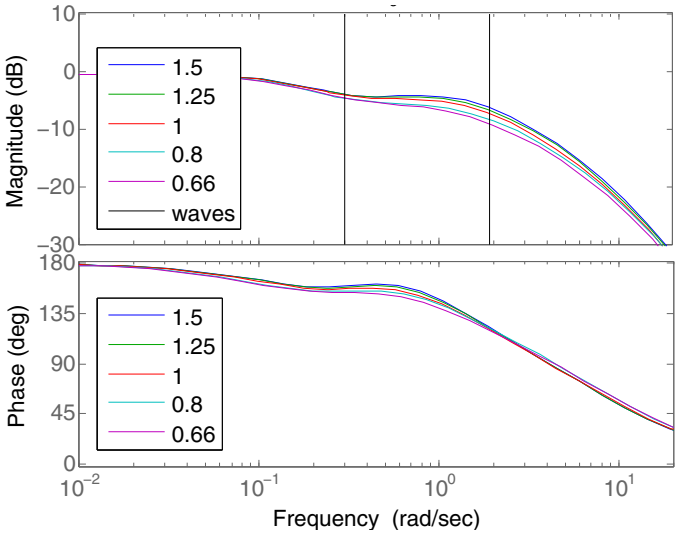

Fig. 5. Bode plot for $\boldsymbol{G}(s)$ for varying gain on the A_{eng} parameter. The gains of (1.5, 1.25, 1, 0.8, 0.66) results in five models representing the model uncertainty. A gain of 1 indicates the nominal model.

2.5 Limitations

Having limited this investigation to feedback from measurement of O_2, the time delay in this measurement imposes a major restriction on the performance of the feedback path of the controller. The approximate upper bound on the cross over frequency of the feedback path is $\omega_c < 1/\tau_d$ (Skogestad and Postlethwaite [1996]). The feedback path hence looses dynamic control authority in proportion to the inverse of time delay. The physical reason to the delay is the low flow rate acceptable by the O_2 sensor. An air flow is obtained by sampling through an orifice. Designed to give nominal flow for the sensor at full load, hence full exhaust pressure, the flow will be smaller at lower engine loads. This load dependency of the time delay is another critical factor for the achievable performance of the feedback path controller.

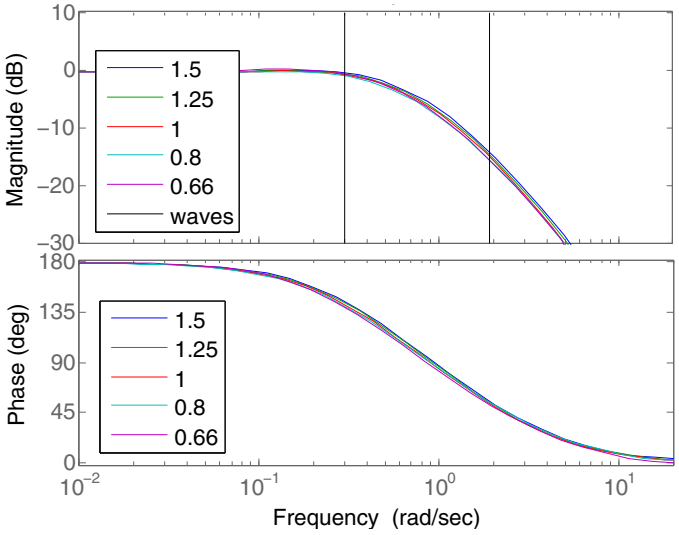

Fig. 6. Bode plot for $\boldsymbol{G}_d(s)$ with varying gain on the A_{eng} model-parameter. A gain of 1 corresponds to the nominal value.

3. CONTROL DESIGN

The control approach here is to combine feed-forward, from fuel index to control input, with feedback from measured O_2. Further, a Smith predictor is employed to alleviate the effects of sensor dead time. The following abbreviations will be used to refer to these control elements:

- Pure feedforward compensation (FF)
- Classical PI feedback from (PI)
- QFT feedback design (QFT)
- Smith predictor (SP)

3.1 Feedforward control

The feedforward control has the advantage of not using the O_{scav} measurement and therefore not being limited by the time delay. The controller, $\boldsymbol{K}_d$, is implemented as suggested in Skogestad and Postlethwaite [1996] see 7.

$$\boldsymbol{K}_d = -\bar{\boldsymbol{G}}^{-1}\bar{\boldsymbol{G}}_d \tag{7}$$

The controller satisfies the criteria listed in Skogestad and Postlethwaite [1996] in order to be perfect. This implies that the controller completely negates the effect of the disturbances, however it relies on a good estimation of the disturbance transfer function, $\boldsymbol{G}_d(s)$. The reference is not controlled and can therefore not be tracked.
The controlled transfer function from disturbance to output is:

$$\frac{y}{d} = \boldsymbol{G}_d + \boldsymbol{K}_d\boldsymbol{G} = \boldsymbol{G}_d - \bar{\boldsymbol{G}}^{-1}\bar{\boldsymbol{G}}_d\boldsymbol{G} \tag{8}$$

Fig. 7 shows the Bode-plots of the controlled model when the model uncertainty from Section 2.4 is introduced as $\boldsymbol{G}$ and $\boldsymbol{G}_d$.

It is clear that the disturbance will be rejected for the wave frequencies even when model uncertainty is introduced. The following controllers investigates the possibilities of aiding the feedforward controller in rejecting the disturbance. All following controllers will employ feedforward.

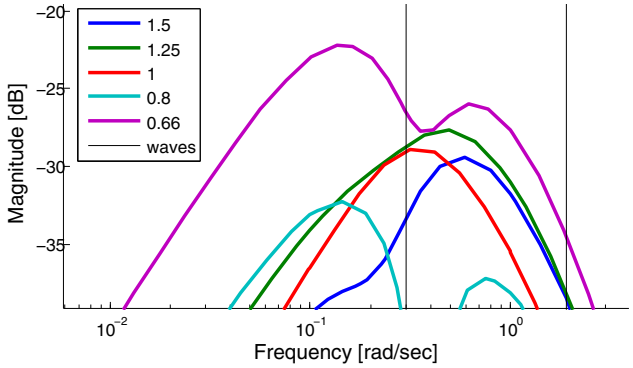

Fig. 7. Bode-plot of FF model with uncertainty transfer functions

3.2 Feedback control - Classical

A feedback controller is designed, to reduce the disturbance effect. A PI-controller is chosen to ensure reference tracking without stationary error.

The time constant of the controller is chosen such that the cut-off frequency is much smaller than the desired cross over frequency. The limitations imposed by the measurement delay restricts the cross over frequency to be less than; $\omega_c < 1/\tau_d = 0.20[rad/s]$. To increase the performance of the controller the time constant is chosen such that the zero introduced by the controller can cancel the slowest pole of $\bar{\boldsymbol{G}}(s)$. The PI-controller is therefore:

$$\boldsymbol{K}_{PI}(s) = \frac{0.98(s+0.19)}{s} \tag{9}$$

which ensures that the cross-over frequency of the controlled model is $0.19[rad/s]$ with a phase margin of 69°.

In Fig. 11 the step responses of the controlled model with uncertainty introduced are depicted as solid lines. The Nichols-plot of the PI controller is shown in Fig. 8.

3.3 Feedback control - QFT

A Quantitative Feedback Theory (QFT) approach is taken to design controllers to be robust towards model uncertainty, while ensuring stability and disturbance rejection.

For the design process a QFT Control Toolbox (QFTCT) from Control & Energy Systems Center is utilised. The toolbox imposes restrictions on the model structure as it is not possible to specify $\bar{\boldsymbol{G}}_d(s)$. The controller design is based on Nichols plots, see Houpis et al. [2006]. The desired stability specification is marked with black in Fig. 8, where the controlled model responses are seen to suffer from a large phase shift due to the measurement delay. The objective in QFT control is to ensure that the model response lies outside the specification area in the Nichols plot, which will ensure good performance in closed loop.

The proposed controller is,

$$\boldsymbol{K}_{QFT}(s) = \frac{0.71(s+0.19)}{s}, \tag{10}$$

where the zero of the controller is in the vicinity of the slowest pole of the model.

Fig. 12 shows the disturbance step responses of the controlled model with uncertainty introduced as solid lines.

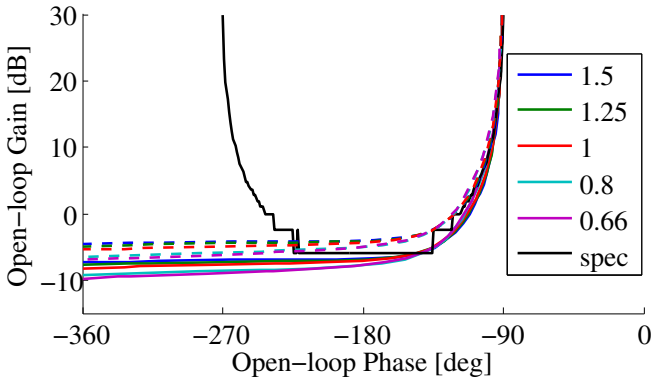

Fig. 8. The PI (dashed) and QFT (solid) controlled open loop Nichols-plot. The gains of (1.5, 1.25, 1, 0.8, 0.66) results in five models representing the model uncertainty. A gain of 1 represents the nominal model.

3.4 Smith predictor

To overcome the effect of the measurement delay and reduce the oscillations on the model responses a Smith predictor, Åstrom et al. [1994], is designed. The Smith predictor relies on a pre-designed controller and introduces an additional feedback from input u to error e, see Fig. 9. The error is expressed in Eq. 11 where K is the pre-designed controller, and $\boldsymbol{G}_{ms} = \left(1 - \hat{\boldsymbol{G}}_m\right)$.

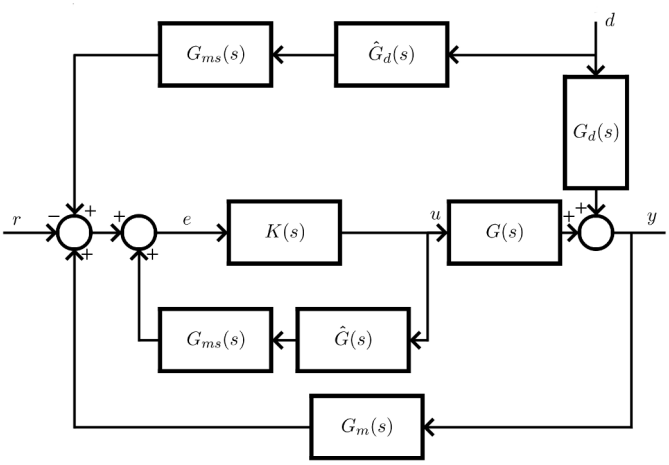

Fig. 9. Controlled model with Smith predictor

$$e = -r + \boldsymbol{G}_m\boldsymbol{G}_d d + \boldsymbol{G}_m\boldsymbol{G}\boldsymbol{K}e + \boldsymbol{G}_{ms}\hat{\boldsymbol{G}}_d d + \boldsymbol{G}_{ms}\hat{\boldsymbol{G}}\boldsymbol{K}e \quad (11)$$

The last term is from the Smith feedback loop where estimates for the measurement, $\bar{\boldsymbol{G}}_m(s)$ and the plant $\bar{\boldsymbol{G}}(s)$ are used to counteract the effect of the measurement delay.

Disturbance simulations using the Smith predictor are carried out. The step responses for the classical and QFT controllers with Smith predictors and feedforward are shown in Fig. 11 and Fig. 12, respectively. In Fig. 10 the step responses for the classical PI is shown without use of feedforaward. All steps are with a 5% increase in disturbance at time $0[s]$.

The oscillatory behaviour is seen to be diminished making it possible for the classically designed controller to control all five model cases.

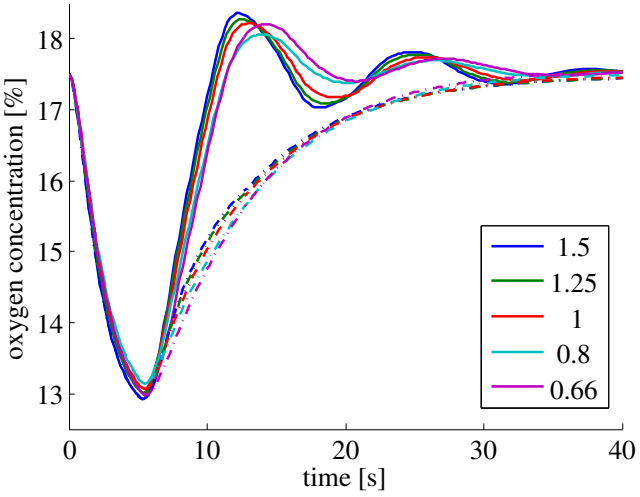

Fig. 10. Disturbance step responses. PI as solid lines and PI with Smith Predictor as dashed lines.

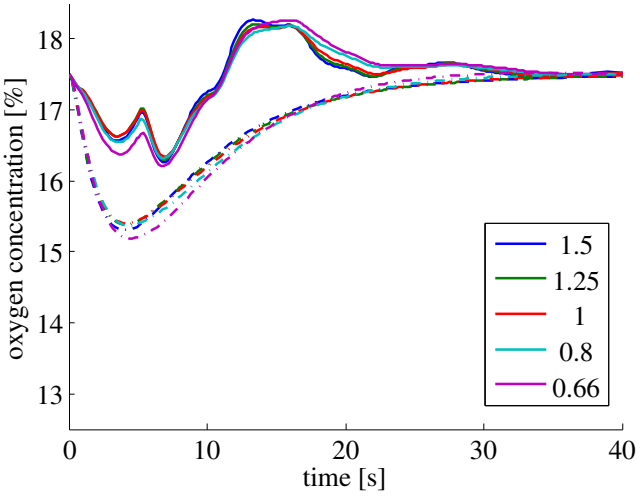

Fig. 11. Disturbance step responses. PI+FF as solid lines and PI+FF with Smith Predictor as dashed lines.

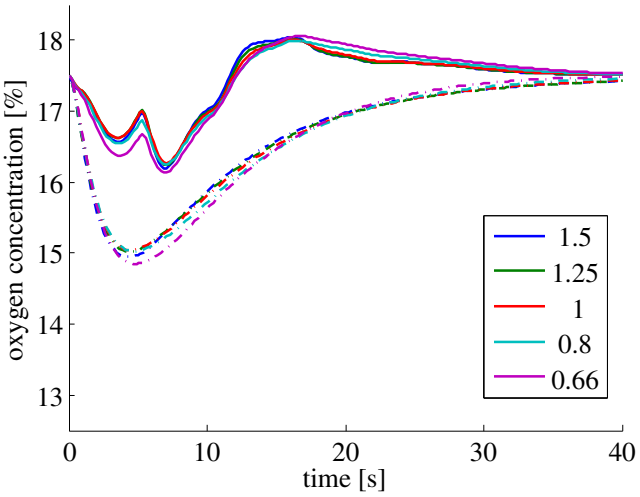

Fig. 12. Disturbance step responses. QFT+FF as solid lines and QFT+FF with Smith Predictor as dashed lines.

The Smith predictor relies on a good estimate of the measurement delay and it is advantageous to design the predictor for a larger measurement delay than expected in order to better reject model uncertainty sensitivity, [Hansen et al., 2013].

Sensitivity The sensitivity of the controlled models with Smith predictor are compared to the sensitivity of the feedforward compensated model in Fig. 13. The top plot is the feedforward compensated model, the bottom plot depicts the sensitivity of the Smith predictor models, where the QFT controlled model is in dashed lines.

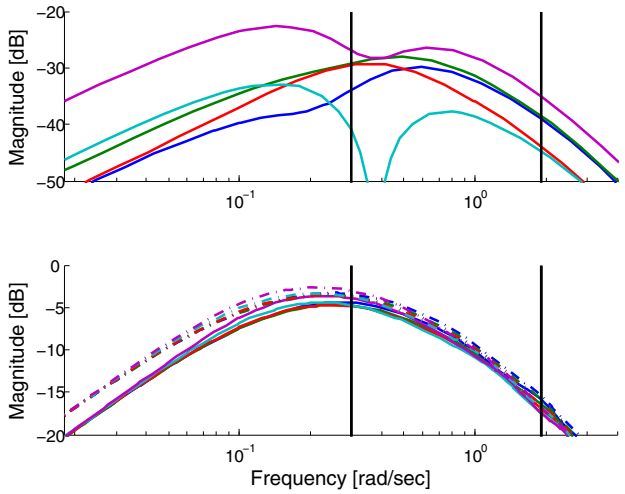

Fig. 13. Sensitivity functions. Top: FF model. Bottom: PI+SP in solid lines and QFT+SP in dashed lines. Colour notation is the same as used in the previous figures.

4. CONCLUSION

With the purpose of NO_x emission reduction from large marine diesel engines, this paper considered exhaust gas recirculation control employing linear classical control concepts. Topologies of feed-forward and feedback control were considered and a Smith predictor was included to alleviate a significant time-delay in the O_2 measurement. Robustness was addressed using variation in parameters in a non-linear model of the process and QFT techniques were employed as an aid to design of robust feedback control. Performance of the EGR control was shown to be satisfactory at low frequencies where current IMO regulations apply, but performance improvement possibilities were shown to be fairly limited if robust sensitivity was a goal under dynamic conditions. The main issues to deal with were shown to be parameter sensitivity of the nonlinear model and the dead time of the primary sensor used for feedback.

REFERENCES

K.J. Åstrom, C.C. Hang, and B.C. Lim. A new smith predictor for controlling a process with an integrator and long dead-time. *IEEE Trans. on Automatic Cont.*, pages 343–345, 1994.

E. Alfieri, A. Amstutz, C. H. Onder, and L. Guzzella. Model-based feedback control of the air-to-fuel ratio in diesel engines based on an empirical model. In *2006 IEEE Int. Conf. on Cont. Appli.*, pages 509 –514, 2006.

P. Chen and J. Wang. Observer-based estimation of air-fractions for a diesel engine coupled with aftertreatment systems. *IEEE Tr. Cont. Syst. Tech.*, pages 1–12, 2012.

G. Colin, P. Lanusse, A. Louzimi, Y. Chamaillard, C. Deng, and D. Nelson-Gruel. Multi-siso robust crone design for the air path control of a diesel engine. *Proc. 18th World Congress, International Federation of Automatic control.*, pages 2254–2259, 2011.

Case Western Reserve Control & Energy Systems Center. The qft control toolbox. `http://cesc.case.edu/OurQFTCT.htm`.

J. M. Hansen, C. G. Zander, N. Pedersen, and M. Blanke. Modelling for control of exhaust gas recirculation on large diesel engines. *IFAC, 9th Conference on Control Application in Marine Systems*, 2013.

C. H. Houpis, S. J. Rasmussen, and M. Garcia-Sanz. *Quantitative Feedback Theory - Fundamentals and applications*. Taylor & Francis, 2006.

P. Kotman, M. Bitzer, and A. Kugi. Flatness-based feedforward control of a diesel engine air system with egr. *IFAC Proceedings Volumes*, pages 598–603, 2010.

S. Skogestad and I. Postlethwaite. *Multivariable Feedback Control*. John Wiley and Sons, 1996.

J. Wahlström and L. Eriksson. Nonlinear egr and vgt control with integral action for diesel engines. *Oil & gas science and technology*, pages 573–586, 2011a.

J. Wahlström and L. Eriksson. Modelling diesel engines with a variable-geometry turbocharger and exhaust gas recirculation by optimization of model parameters for capturing non-linear system dynamics. *Proc. Inst. of Mechanical Engineers. Part D, Journal of Automobile Engineering*, pages 960–986, 2011b.

H. P. Wang, J. Bosche, Y. Tian, and A. El Hajjaji. Two loop based dynamical feedback stabilization control of a diesel engine with egr and vgt. *Proc. IEEE Conf on Decision and Control*, pages 1596–1603, 2011a.

Y. Wang, I. Haskara, and O. Yaniv. Quantitative feedback design of air and boost pressure control system for turbocharged diesel engines. *Control Engineering Practice*, pages 626–637, 2011b.

Appendix A. NOMENCLATURE

Table A.1. Nomenclature

General	$\dot{m}$	Mass flow
	ω	Rotational speed
	O	Oxygen concentration
	p	Pressure
$\boldsymbol{u}, \boldsymbol{d}, y$	ω_{blow}	Rotational speed of blower
	u_{egr}	Opening signal for COV
	u_{load}	Engine load
	u_{vgt}	Opening signal for VGT
	O_{scav}	Scavenge oxygen concentration
States	p_{scav}	Scavenge manifold pressure
	p_{exh}	Exhaust manifold pressure
	p_{blow}	Pressure in EGR plenum
	O_{scav}	Scavenge oxygen concentration
	O_{exh}	Exhaust oxygen concentration
	ω_t	Turbocharger rotational speed
	$\tilde{u}_{vgt}$	Dynamics of u_{vgt}
	$T_{1,k}$	Internal engine temperature
	$x_{r,k}$	Gas fraction in engine